The Synthesis of Three-Degree-of-Freedom Planar Parallel Manipulators with Revolute Joints (3-RRR) for an Optimal Singularity-Free Workspace

Marc Arsenault
Roger Boudreau
e-mail : boudrer@umoncton.ca
Faculté d'ingénierie, Université de Moncton, Moncton, New Brunswick, Canada, E1A 3E9

Abstract: In this paper, a method is presented for the synthesis of 3-RRR manipulators. The method uses a genetic algorithm while considering three different design criteria: the optimization of the manipulator workspace to approach a prescribed workspace, the maximization of the manipulator's dexterity and the avoidance of singularities inside the manipulator workspace. It is shown that, for a given manipulator, some working modes do not have any corresponding singularity curves located inside the manipulator workspace. Furthermore, a case is presented where, for a given orientation range of the manipulator's mobile platform, there are no parallel singularities located inside the workspace.

Résumé: Cet ouvrage présente une méthode de synthèse pour les manipulateurs 3-RRR. La méthode se base sur l'utilisation d'un algorithme génétique en considérant trois différents critères de conception: l'optimisation de l'espace atteignable du manipulateur pour approcher un espace prescrit, la maximisation de la dextérité du manipulateur ainsi que l'évitement de la présence de singularités dans son espace atteignable. Il est démontré que, pour un manipulateur quelconque, il est possible que certains modes de fonctionnement n'aient pas de courbes singulières correspondantes à l'intérieur de l'espace atteignable du manipulateur. En fait, un cas est présenté dans lequel il n'y a pas de courbes singulières dans l'espace atteignable du manipulateur pour plusieurs orientations de sa plate-forme mobile.

1. INTRODUCTION

It is a well known fact that the design of parallel manipulators is less intuitive than that of their serial counterparts. One reason for this is the increased number of parameters needed to define this type of manipulator. Furthermore, several of the criteria used during the design phase are of a contradictory nature thus making their optimization a difficult exercise. Therefore, numerous design methods have been developed by researchers to aid the designers of parallel manipulators[1~4]. Many of these methods use the manipulator's workspace as well as its kinematic properties as design criteria.

In this paper, a design method is presented for a general three-degree-of-freedom (3-DOF) planar parallel manipulator with revolute joints in which the first joint of each chain is actuated (3-RRR). The interesting property of this manipulator is that its revolute actuators are attached to the base thus reducing the inertia of its mobile parts. The design criteria used in this work are the manipulator's workspace, dexterity and singularities.

Previous studies of the singularities of the 3-RRR manipulator are quite recent. Gosselin and Wang[5] were apparently the first researchers to attempt the determination of these singularities.

They derived a high degree polynomial corresponding to all of the singularities of the 3-RRR manipulator. Afterwards, this work was revised by Bonev and Gosselin[6] who succeeded in reducing the degree of the polynomial to a minimal value. Both of these papers contained a graphical representation of the singularity loci using a discretization approach.

To the authors' knowledge, no prior research has been done on the optimization of the 3-RRR manipulator while trying to avoid the presence of singularities inside the workspace. In this work, the singularity criterion is combined with the optimization of the workspace to approach a prescribed workspace, as well as with the maximization of the manipulator's dexterity. The goal of the synthesis is to obtain a manipulator suitable for a specified task.

Because of the apparent complexity of the manipulator synthesis, a genetic algorithm is chosen as the optimization method due to its good convergence properties. Genetic algorithms have been used by several researchers in the design and optimization of parallel manipulators[7~9]. Specifically, the work of Gallant and Boudreau[10] is mentioned here since it shares many of the objectives of this paper.

The results section of this work concentrates on demonstrating the ability of the method to consistently converge towards acceptable solutions. An effort is also made to emphasize the beneficial effect of dexterity optimization. Finally, an interesting result regarding the 3-RRR manipulator's singularities is presented.

2. GEOMETRIC DESCRIPTION OF A 3-RRR MANIPULATOR

A general 3-DOF planar parallel manipulator with revolute joints is shown in Figure 1. It consists of a triangular mobile platform, $B_1B_2B_3$, and a fixed base, $O_1O_2O_3$, joined by three kinematic chains. Each kinematic chain is formed by a proximal link, O_iA_i, and a distal link, A_iB_i with the joints located at O_i, A_i, and B_i being of the revolute type (in this paper i = 1, 2, 3). The length of the proximal links is l_1, while l_2 is the length of the distal links. The vectors along lines OO_i, O_iA_i, O_iB_i, and $O'B_i$ are represented by $\boldsymbol{o}_i$, $\mathbf{u}_i$, $\boldsymbol{r}_i$, and $\boldsymbol{s}_i$, respectively.

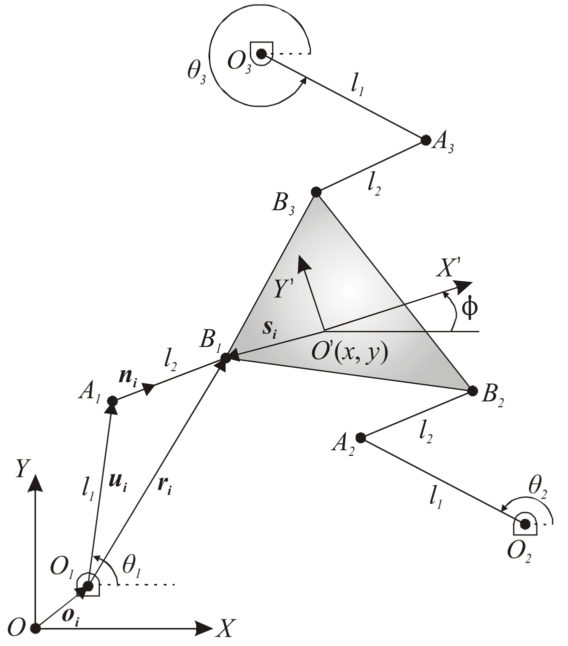

Figure 1 Three-degree-of-freedom planar parallel manipulator with revolute joints

We first define a coordinate system fixed to the base of the manipulator, called the *base frame*, with center O and axes X and Y. Similarly, we then define a coordinate system fixed to the mobile platform, called the *mobile frame*, with center O' and axes X' and Y'. Henceforth, the superscript $'$ will be used to denote vectors expressed in the mobile frame whereas no superscript will be used when expressing vectors in the base frame. The *pose* (the position and orientation) of the mobile platform, expressed relative to the base frame by the position vector $\boldsymbol{v} = [x,y]^{\mathrm{T}}$ and the angle ϕ, can be modified by the revolute actuators located at points O_i. The output $\boldsymbol{x}$ of the manipulator is thus:

$$\boldsymbol{x} = [x, y, \phi]^{\mathrm{T}} \tag{1}$$

Conversely, the input $\boldsymbol{\varphi}$ of the manipulator is represented by the angular positions of the revolute actuators (θ_i) measured from the X axis to each of the proximal links:

$$\boldsymbol{\varphi} = [\theta_1, \theta_2, \theta_3]^{\mathrm{T}} \tag{2}$$

The 14 variables to be optimized during the manipulator synthesis are: O_{1x}, O_{1y}, O_{2x}, O_{2y}, O_{3x}, O_{3y}, B'_{1x}, B'_{1y}, B'_{2x}, B'_{2y}, B'_{3x}, B'_{3y}, l_1, l_2.

3. WORKSPACE DETERMINATION AND OPTIMIZATION

Many definitions exist for the workspace of parallel manipulators[11~12]. In this paper, the constant orientation workspace is chosen. This type of workspace corresponds to the set of positions reachable by the mobile platform as it translates in a plane at a fixed orientation.

3.1 Workspace Determination

The geometrical method[13] will be used here for the determination of the manipulator's workspace. With this method, the constant orientation workspace of a planar parallel manipulator can be found as the intersection of annular regions corresponding to the reachable workspaces of its kinematic chains.

Based on the definitions provided in the previous section, the following equation can be written representing the vectors joining points O_i and B_i:

$$\boldsymbol{r}_i = \boldsymbol{v} + \boldsymbol{R}\boldsymbol{s}_i' - \boldsymbol{o}_i \tag{3}$$

In the above expression, $\boldsymbol{R}$ is a 2x2 rotation matrix representing the orientation of the mobile system relative to the base system. The annular regions corresponding to the reachable workspaces of the kinematic chains are defined by pairs of concentric circles with radii equal to the maximum and minimum amplitudes of $\boldsymbol{r}_i$. The expression for the amplitude of $\boldsymbol{r}_i$ can be obtained from Eq. (3):

$$\|\boldsymbol{r}_i\| = \sqrt{\left\{\begin{bmatrix} x \\ y \end{bmatrix} + \begin{bmatrix} \cos\phi & -\sin\phi \\ \sin\phi & \cos\phi \end{bmatrix}\begin{bmatrix} B_{ix}' \\ B_{iy}' \end{bmatrix} - \begin{bmatrix} O_{ix} \\ O_{iy} \end{bmatrix}\right\}^T \left\{\begin{bmatrix} x \\ y \end{bmatrix} + \begin{bmatrix} \cos\phi & -\sin\phi \\ \sin\phi & \cos\phi \end{bmatrix}\begin{bmatrix} B_{ix}' \\ B_{iy}' \end{bmatrix} - \begin{bmatrix} O_{ix} \\ O_{iy} \end{bmatrix}\right\}} \tag{4}$$

Also, from Figure 1, it can easily be seen that:

$$\|\boldsymbol{r}_i\|_{\min/\max} = |\, l_1 \pm l_2 \,| \tag{5}$$

which corresponds to the configurations where the proximal and distal links are aligned. Squaring the right hand sides of Eqs. (4) and (5), we obtain, after simplification :

$$(l_1 \pm l_2)^2 = \left(x + B_{ix}' \cos\phi - B_{iy}' \sin\phi - O_{ix}\right)^2 + \left(y + B_{ix}' \sin\phi + B_{iy}' \cos\phi - O_{iy}\right)^2 \tag{6}$$

The centers of the circles defined by Eq. (6) are expressed as:

$$\begin{aligned} a_i &= -B_{ix}' \cos\phi + B_{iy}' \sin\phi + O_{ix} \\ b_i &= -B_{ix}' \sin\phi - B_{iy}' \cos\phi + O_{iy} \end{aligned} \tag{7}$$

For a constant orientation of the mobile platform, the centers of the circles are fixed and three pairs of concentric circles are obtained. The workspace consists of the intersection of these regions. In some cases, the intersection of the annular regions is composed of two or more closed areas. When this situation occurs, only one of the areas is selected for use in the optimization process since the manipulator cannot move from one area to another without being reassembled.

3.2 Workspace Optimization

The first optimization goal in this work is to obtain an actual manipulator workspace that resembles as much as possible a prescribed workspace. Figure 2 shows an actual workspace (R_a) and a prescribed workspace (R_p). The intersection of the workspaces is defined as $R_i = R_a \cap R_p$. The sections of both workspaces, actual and prescribed, that do not intersect are $R'_a = R_a - R_i$ and $R'_p = R_p - R_i$, respectively. The sum of R'_a and R'_p represents the error on the actual workspace. The area of the error, computed with the Gauss-Divergence theorem, is minimized in the optimization cycle[14].

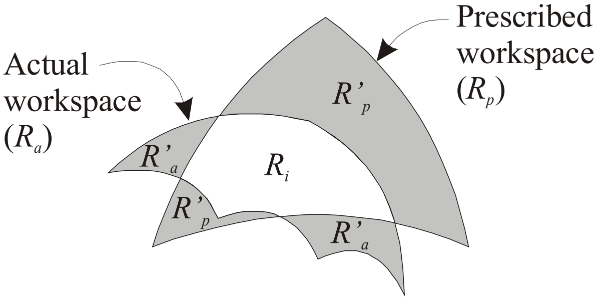

Figure 2 Prescribed and actual workspaces with identification of the regions

In some cases, it might be necessary to have the manipulator be capable of reaching the entire prescribed workspace. Although no results are presented here, this can be accomplished by applying a condition in the algorithm verifying that the prescribed workspace is located entirely inside the actual workspace.

4. JACOBIAN MATRIX DETERMINATION

In this section, the analytical development of the manipulator's Jacobian matrix is presented. The formulation used is primarily taken from Bonev and Gosselin[6].

We begin by defining unit vectors $\boldsymbol{n}_i$ directed along the distal links. The following relation can thus be obtained for each kinematic chain:

$$l_2\boldsymbol{n_i} = \boldsymbol{v} + \boldsymbol{Rs_i}' - \boldsymbol{u_i} - \boldsymbol{o_i} \tag{8}$$

By squaring both sides of Eq. (8) and applying the law of cosines:

$$l_2^2 = (\boldsymbol{v} + \boldsymbol{Rs_i}' - \boldsymbol{u_i} - \boldsymbol{o_i})^{\mathrm{T}}(\boldsymbol{v} + \boldsymbol{Rs_i}' - \boldsymbol{u_i} - \boldsymbol{o_i}) \tag{9}$$

$$l_2^2 = \|\boldsymbol{r_i}\|^2 + l_1^2 - 2\boldsymbol{r_i}^{\mathrm{T}}\boldsymbol{u_i} \tag{10}$$

Furthermore, from Figure 1, it is seen that:

$$\boldsymbol{u_i} = l_1\begin{bmatrix}\cos\theta_i \\ \sin\theta_i\end{bmatrix} \tag{11}$$

From Eqs. (3) and (7), the following is also obtained:

$$\boldsymbol{r_i} = \begin{bmatrix}x - a_i \\ y - b_i\end{bmatrix} \tag{12}$$

Now, since a_i and b_i are constants for a given orientation of the mobile platform, Eq. (10) can be rewritten as:

$$\cos\theta_i(x-a_i)+\sin\theta_i(y-b_i)=\frac{(x-a_i)^2+(y-b_i)^2+l_1^{\,2}-l_2^{\,2}}{2l_1}\equiv p_i \tag{13}$$

The previous equation establishes a relation between the input variables ($\boldsymbol{\varphi}$) and the output variables ($\boldsymbol{x}$) of the manipulator. For a real solution to Eq. (13) to exist, the following condition needs to be satisfied:

$$(x-a_i)^2+(y-b_i)^2-p_i^{\,2}\equiv\Gamma_i\geq 0 \tag{14}$$

If $\Gamma_i > 0$, two solutions exist to Eq. (13) as expressed in the following:

$$\sin\theta_i=\frac{p_i(y-b_i)+(x-a_i)\delta_i\sqrt{\Gamma_i}}{\rho_i}\quad,\quad \cos\theta_i=\frac{p_i(x-a_i)-(y-b_i)\delta_i\sqrt{\Gamma_i}}{\rho_i} \tag{15a}$$

$$\theta_i=\arctan 2\left(\frac{\sin\theta_i}{\cos\theta_i}\right) \tag{15b}$$

where $\rho_i = ||\boldsymbol{r_i}||^2$ and $\delta_i = \pm 1$. Eq. (15a) is not valid if $\rho_i = 0$, which may occur only when $l_1 = l_2$ and $B_i \equiv O_i$.

The solutions presented in Eq. (15) correspond to the two possible configurations of each kinematic chain for a given manipulator posture. Consequently, $\boldsymbol{\Delta_j} = [\delta_1, \delta_2, \delta_3]$ is established as the working mode index (j = 1,2,…,8). The working modes of a 3-RRR manipulator, as defined by Chablat and Wenger[15], identify the different solutions to its inverse kinematic problem (IKP). Since there are potentially 8 different solutions to the IKP of a 3-RRR manipulator, $\boldsymbol{\Delta_j}$ can take the following values:

$$\begin{array}{ll}\boldsymbol{\Delta_1} = [1, 1, 1] & \boldsymbol{\Delta_5} = [-1, -1, -1]\\ \boldsymbol{\Delta_2} = [-1, 1, 1] & \boldsymbol{\Delta_6} = [1, -1, -1]\\ \boldsymbol{\Delta_3} = [1, -1, 1] & \boldsymbol{\Delta_7} = [-1, 1, -1]\\ \boldsymbol{\Delta_4} = [1, 1, -1] & \boldsymbol{\Delta_8} = [-1, -1, 1]\end{array} \tag{16}$$

In order to obtain the Jacobian matrix, we first calculate the derivative of Eq. (9) with respect to time:

$$l_2\boldsymbol{n_i}^T\left(\begin{bmatrix}\dot{x}\\ \dot{y}\end{bmatrix}+\dot{\phi}\,\boldsymbol{Es_i}-l_1\,\dot{\theta}_i\begin{bmatrix}-\sin\theta_i\\ \cos\theta_i\end{bmatrix}\right)=0 \tag{17}$$

where $\boldsymbol{E}$ is equivalent to $\boldsymbol{R}$ evaluated at $\boldsymbol{\phi} = \pi/2$ and:

$$\boldsymbol{s_i}=\begin{bmatrix}-a_i+O_{ix}\\ -b_i+O_{iy}\end{bmatrix}\equiv\begin{bmatrix}c_i\\ d_i\end{bmatrix} \tag{18}$$

By manipulating Eq. (17) and expressing it in vector form, the following expression can be found:

$$\begin{bmatrix}l_2\boldsymbol{n_i}^T & l_2\boldsymbol{n_i}^T\boldsymbol{Es_i}\end{bmatrix}\dot{\boldsymbol{x}}-l_1l_2\boldsymbol{n_i}^T\begin{bmatrix}-\sin\theta_i\\ \cos\theta_i\end{bmatrix}\dot{\theta}_i=0 \tag{19}$$

where:

$$l_2\boldsymbol{n_i}=\begin{bmatrix}x-a_i-l_1\cos\theta_i\\ y-b_i-l_1\sin\theta_i\end{bmatrix} \tag{20}$$

Finally, by combining Eqs. (15a) and (19), we get the following expression:

$$\left[l_2 \boldsymbol{n_i}^T \quad l_2 \boldsymbol{n_i}^T \boldsymbol{Es_i}\right]\dot{\boldsymbol{x}} + l_1 \delta_i \sqrt{\Gamma_i}\,\dot{\theta}_i = 0 \tag{21}$$

which can be expressed in matrix form as:

$$\begin{bmatrix} l_2\boldsymbol{n}_1^T & l_2\boldsymbol{n}_1^T\boldsymbol{Es_I} \\ l_2\boldsymbol{n}_2^T & l_2\boldsymbol{n}_2^T\boldsymbol{Es}_2 \\ l_2\boldsymbol{n}_3^T & l_2\boldsymbol{n}_3^T\boldsymbol{Es}_3 \end{bmatrix}\dot{\boldsymbol{x}} + l_1\begin{bmatrix} \delta_1\sqrt{\Gamma_1} & 0 & 0 \\ 0 & \delta_2\sqrt{\Gamma_2} & 0 \\ 0 & 0 & \delta_3\sqrt{\Gamma_3} \end{bmatrix}\dot{\varphi} = \boldsymbol{J}_x\,\dot{\boldsymbol{x}} + \boldsymbol{J}_\varphi\,\dot{\varphi} = 0 \tag{22}$$

In the above expression, $\boldsymbol{J_x}$ and $\boldsymbol{J_\varphi}$ are the manipulator's 3x3 Jacobian matrices. These matrices can be combined to obtain a single Jacobian matrix that establishes the inverse transformation between the input and output velocities:

$$\boldsymbol{J} = \text{-}\boldsymbol{J_\varphi}^{-1}\boldsymbol{J_x} \tag{23}$$

5. SINGULARITY ANALYSIS

The singularities of parallel manipulators have been studied extensively by Gosselin and Angeles[16]. From this study, two main types of singularities may occur: serial and parallel. Serial singularities (det($\boldsymbol{J_\varphi}$) = 0) occur at the boundaries of the workspace when $\Gamma_i = 0$, and are already considered during workspace determination. On the other hand, parallel singularities (det($\boldsymbol{J_x}$) = 0) correspond to manipulator configurations in which the three distal links are either parallel or intersect at a single point. These singularities are considered during the design process since they may be located inside the manipulator workspace where they would cause significant control problems.

From Eqs. (21) and (22), it can be seen that $\boldsymbol{J_x}$ is a function of Δ_j. Consequently, a different Jacobian matrix (and thus a different set of singularities) exists for each working mode of the manipulator. In order to show the complexity of the singularity curves, an example of a 3-<u>R</u>RR manipulator studied in [6] is shown in Figures 3 and 4. In the latter, the singularities associated with each working mode are shown separately.

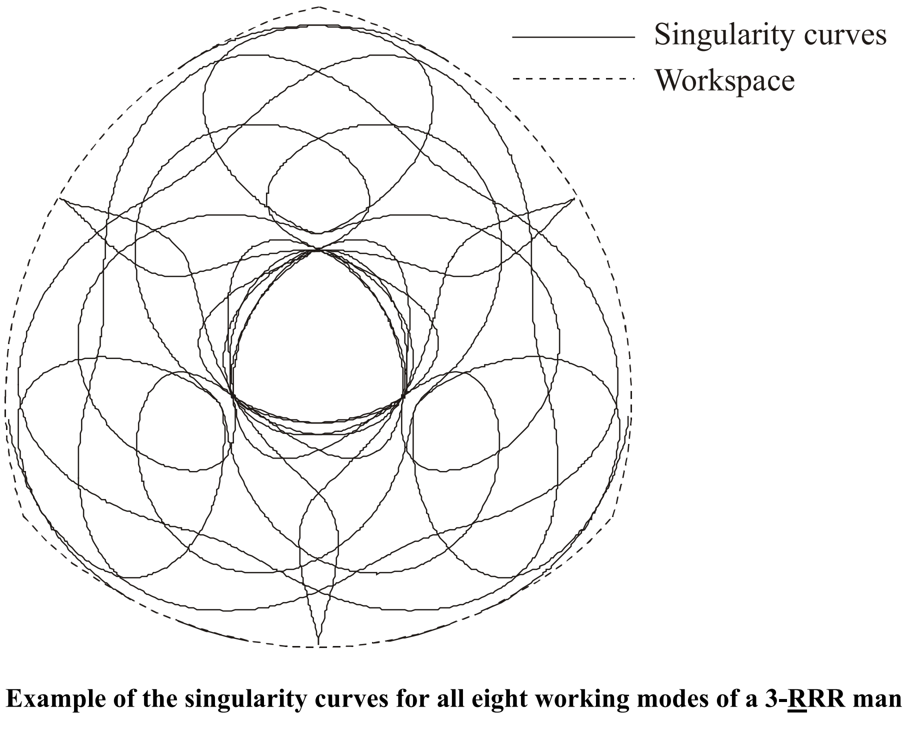

Figure 3 Example of the singularity curves for all eight working modes of a 3-<u>R</u>RR manipulator

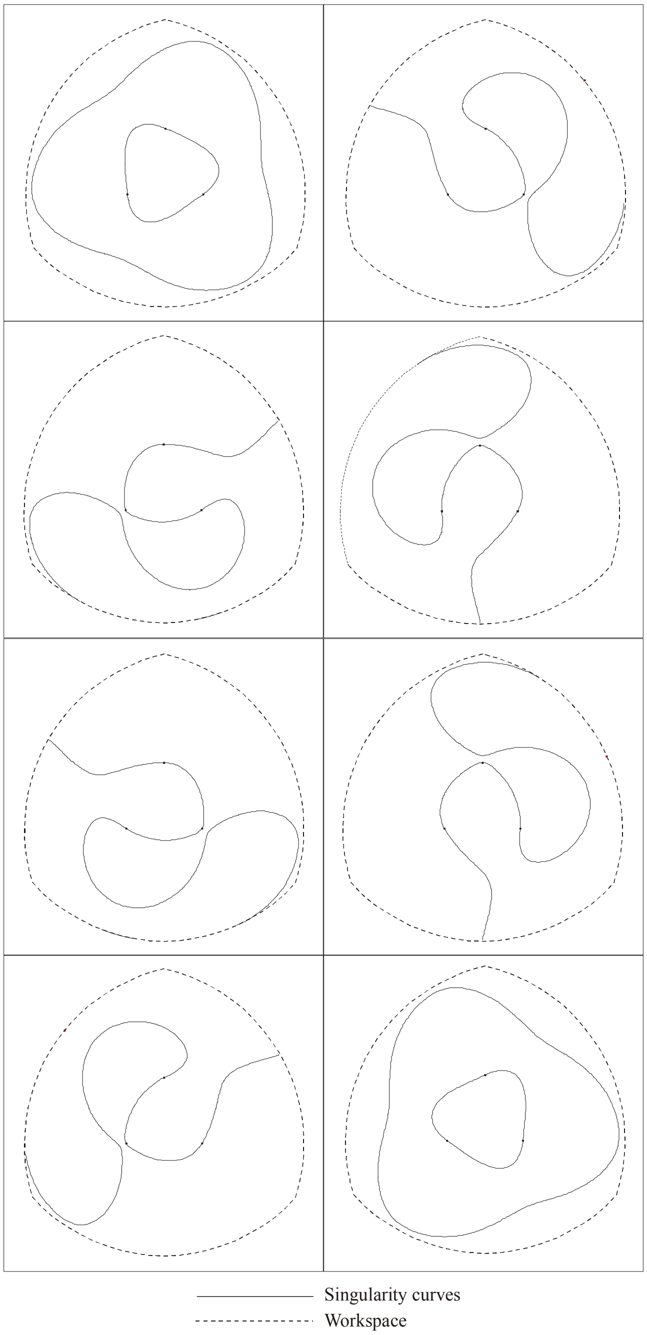

Figure 4 Example of singularity curves for a 3-$\underline{\text{R}}$RR manipulator's individual working modes

Since the expression for det($\boldsymbol{J_x}$) contains radical terms ($\sqrt{\Gamma_i}$), the analytical determination of the singularities for each working mode is impossible. Bonev and Gosselin[6] succeeded in eliminating the radicals by combining the equations for each working mode. The result is a polynomial of degree 42 in X and Y representing the singularities of all working modes. In spite of this, the size and complexity of this expression make the algebraic manipulation of the singularities very difficult. Therefore, the determination of the parallel singularities and the verification of their presence inside the manipulator workspace are accomplished using numerical methods.

5.1 Singularity Determination

The determination of the parallel singularities consists in finding the set of positions in the manipulator's workspace where the determinant of $\boldsymbol{J_x}$ is null. In order to achieve this, we proceed to a discretization of the workspace, thus obtaining a set of points at which the determinant of $\boldsymbol{J_x}$ is evaluated. Singular positions are found when a sign change of det($\boldsymbol{J_x}$) occurs between consecutive points. With the objective of finding the singularities with greater accuracy while maintaining a reasonable search time, the workspace points are swept along both the X and Y axes. Furthermore, a coarse discretization is used as a primary sweep and, when a sign change is found between consecutive points, the workspace between these points is further divided during a secondary sweep. Once an array of singular points has been found, an algorithm similar to the modified gift wrapper algorithm[17] is used to sort and divide the points into singularity curves which can then be plotted. This procedure is repeated for each of the manipulator's eight working modes ($\boldsymbol{\Delta_j}$).

5.2 Singularity Avoidance

It is essential for a parallel manipulator's workspace to be free of singularities since near these configurations, the control of the mobile platform becomes very difficult. Consequently, during the optimization process, the workspace of each manipulator that is encountered needs to be verified for the presence of singularities.

In this paper, it is supposed that the manipulator will operate in one working mode only. In the case of the 3-$\underline{\text{R}}$RR manipulator, this implies that the mobile platform will never be allowed to reach the workspace boundaries during its operation. Situations in which working mode changes may occur are thus avoided. Furthermore, this does not represent a great limitation to the operation of the manipulator since its dimensions can always be scaled to obtain a workspace slightly larger than the task area. Because of this condition, only the singularities relating to one of the eight working modes of the manipulator need to be avoided.

The task of verifying the presence of singularities in the manipulator's workspace is complicated by the fact that an analytical method cannot be used. Moreover, because the procedure must be repeated many times during the optimization process, methods based on the discretization of the workspace would be very time-consuming. Therefore, a method based on the discretization of the workspace boundaries is chosen. This method assumes that all of the singularity curves intersect the workspace boundary. In fact, this hypothesis is not entirely valid, as closed singularity curves located entirely inside the workspace are possible. However, since this situation occurs rarely, the optimization process considers only singularity curves that intersect the workspace boundary. Once a manipulator is found, a visual inspection of the singularities of the optimized manipulator is conducted to ensure no closed singularities are within the workspace. In fact, in the 120 simulations that were run, approximately 5% contained closed singularities located entirely inside the workspace.

The discretization of the workspace boundary is simple since the latter is expressed as a set of circular arcs. The determinant of $\boldsymbol{J_x}$ can thus be evaluated at points on the arcs separated by specified angle increments. As soon as a sign change of det($\boldsymbol{J_x}$) occurs between consecutive points, the presence of singularities inside the manipulator's workspace is confirmed.

6. DEXTERITY OPTIMIZATION

The dexterity can be considered as the ability of the manipulator to perform small displacements at a specified pose of its workspace. It is based on the condition number of the Jacobian matrix:

$$\kappa = \frac{\sigma_{\max}}{\sigma_{\min}} \tag{24}$$

where $\sigma_{\max}$ and $\sigma_{\min}$ represent the maximum and minimum singular values of $\boldsymbol{J}$, respectively. Since κ can reach values from 1 to ∞, $\eta = 1/\kappa$ is used, bounding the dexterity between 0 and 1 where a value of unity represents a perfectly isotropic matrix.

To compute the condition number of a matrix with Eq. (24), an ordering of the singular values of the matrix is required. However, since the 3-$\underline{\text{R}}$RR manipulator is used for both positioning and orienting tasks, the entries of its Jacobian have different units, making such an ordering impossible. Therefore, the Jacobian matrix needs to be modified to render its units homogeneous.

The approach used here is very similar to the one proposed by Gosselin[18]. The method consists of expressing the position and orientation of the manipulator's mobile platform with the Cartesian coordinates of three points on the platform (*C*, *D*, and *E*) instead of with the current output vector $\boldsymbol{x} = [x, y, \phi]^{\mathrm{T}}$. By doing this, the vector of output velocities becomes:

$$\dot{\mathbf{x}}' = \left[v_{cx}, v_{cy}, v_{dx}, v_{dy}, v_{ex}, v_{ey}\right]^T \tag{25}$$

where $\mathbf{v}_c = \left[v_{cx}, v_{cy}\right]^T$, $\mathbf{v}_d = \left[v_{dx}, v_{dy}\right]^T$, and $\mathbf{v}_e = \left[v_{ex}, v_{ey}\right]^T$ are the Cartesian velocities of points *C*, *D*, and *E*, respectively. The relationship between the output and the input velocities changes to:

$$\dot{\boldsymbol{x}}' = \boldsymbol{J}' \dot{\varphi} \tag{26}$$

where $\dot{\mathbf{x}}' = \mathbf{S}\dot{\mathbf{x}}$, $\mathbf{J}' = \mathbf{S}\,\mathbf{J}^{-1}$ and:

$$\mathbf{S} = \begin{bmatrix} 1 & 0 & -\left(x_c \sin\phi + y_c \cos\phi\right) \\ 0 & 1 & \left(x_c \cos\phi - y_c \sin\phi\right) \\ 1 & 0 & -\left(x_d \sin\phi + y_d \cos\phi\right) \\ 0 & 1 & \left(x_d \cos\phi - y_d \sin\phi\right) \\ 1 & 0 & -\left(x_e \sin\phi + y_e \cos\phi\right) \\ 0 & 1 & \left(x_e \cos\phi - y_e \sin\phi\right) \end{bmatrix} \tag{27}$$

In the above equation, $\mathbf{p}_c = \left[x_c, y_c\right]^T$, $\mathbf{p}_d = \left[x_d, y_d\right]^T$ and $\mathbf{p}_e = \left[x_e, y_e\right]^T$ are the position vectors of points *C*, *D*, and *E*. It can be noted that $\mathbf{S}$ will not introduce singularities in the velocity relationship as long as the chosen points are distinct. The dexterity of the manipulator can then be estimated by the condition number of $\boldsymbol{J}'$ whose entries have all the same units.

The choice of points *C*, *D*, and *E* has a direct influence on the value of the conditioning of $\boldsymbol{J}'$ and can induce errors in the comparison of the dexterity of different manipulators. It was found by Kim[19] that the points yielding the lowest condition number for $\boldsymbol{J}'$ are set on the vertices of an equilateral triangle centered at the centroid of the mobile platform's attachment points (B_1, B_2, B_3). Furthermore, it was found that, for optimal dexterity, the sides of this triangle should be in the same order of length as the size of the platform. Also, since the orientation of the triangle does not affect the conditioning, the selection of the points need not take into account the orientation of the mobile platform. In this work, points *C*, *D*, and *E* were thus chosen on an equilateral triangle centered at the centroid of the mobile platform with sides having a length equal to the maximal distance between each of the platform's attachment points and its centroid.

Since the dexterity (η) is a local property of the manipulator, a global conditioning index (GCI) was introduced by Gosselin and Angeles[20] to measure the former throughout the manipulator's workspace. The GCI is computed by discretizing the workspace, calculating η at each point obtained and then computing its average over the workspace.

Since the Jacobian is dependant on the manipulator's active working mode, so will the GCI. Consequently, during the optimization process, the GCI is computed for each of the manipulator's eight working modes (Δ_j) with the goal of finding the one for which it is maximized. However, before evaluating the GCI for a particular working mode, the presence of singularities corresponding to this working mode inside the manipulator's workspace is verified. If singularities are present inside the workspace, the GCI is not computed for the corresponding working mode since the solution is not acceptable.

7. GENETIC ALGORITHM

A genetic algorithm is a non-traditional optimization method based on the Darwinian survival-of-the-fittest evolutionary theory. The method is based on the creation and evolution of many individuals that, through several generations, become stronger.

Each randomly created individual represents a set of manipulator parameters. The strength of these individuals is evaluated using an objective function based on the optimization goals of the manipulator: error on the workspace area, singularity avoidance, and dexterity. The evolution of the individuals is accomplished using genetic operators such as selection, crossover and mutation until the method converges towards an optimal solution. A real-coded genetic algorithm is used in this work since it has been shown[21] that this type of algorithm has a better performance than a binary-coded one. In this work, a population of 100 individuals was optimized using a maximum of 100 generations.

8. RESULTS

One of the design criteria used in this work is for the optimized manipulator to have at least one working mode that doesn't have any corresponding singularity curves located inside the workspace. The results presented in this section show that this criteria can be satisfied. However, since this work seems to be the first that succeeds in optimizing the 3-$\underline{R}$RR manipulator while considering singularity avoidance, it is also interesting to note that some manipulators, for all working modes, do not have any singularity curves located inside their workspace for several different orientations of their mobile platform. One such manipulator is shown in Figure 5a and its geometrical parameters are listed in Table 1. It was found that this manipulator does not have any parallel singularities inside its workspace for orientations varying from -90 to +90 degrees. The workspace of the manipulator for several orientations is shown in Figure 5b.

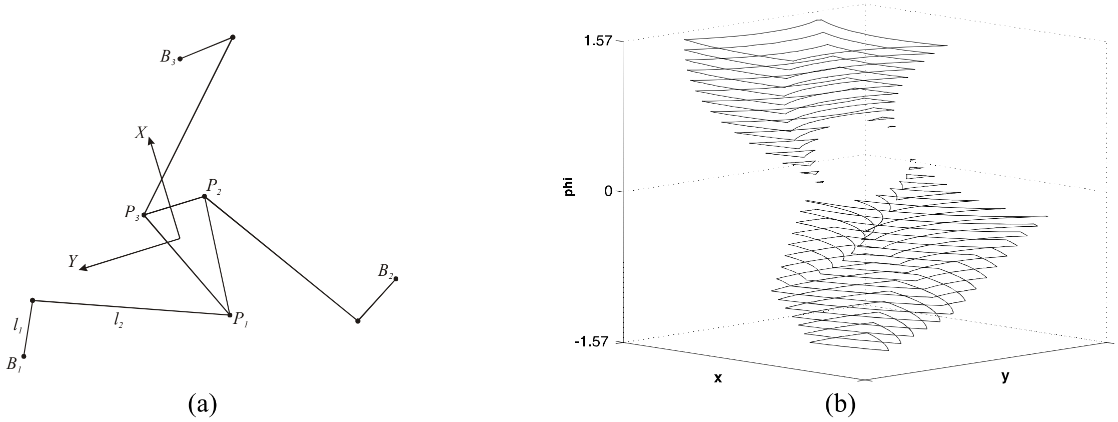

(a) (b)

Figure 5 (a) Manipulator geometry (b) Manipulator workspace for orientations ranging from -90 to +90 degrees

Table 1 Geometric parameters of the singularity-free manipulator shown in Figure 5

B_{1x}	-13.29	B_{1y}	-11.25	P_{1x}	-5.75	P_{1y}	-1.69	l_1	3.75
B_{2x}	11.32	B_{2y}	-6.15	P_{2x}	2.16	P_{2y}	-2.34	l_2	13.05
B_{3x}	-2.92	B_{3y}	8.32	P_{3x}	2.20	P_{3y}	1.80		

The optimized manipulators presented in this section are found by minimizing one of the following objective functions to evaluate the individuals in the genetic algorithm:

$$ObjFun = \alpha + \tau \cdot w_1 \tag{28}$$

$$ObjFun = \alpha + \tau \cdot w_1 + (1 - \beta) \cdot w_2 \tag{29}$$

In the previous equations, α is the error on the workspace, τ is a binary variable representing the presence of singularities in the workspace, β is the GCI, w_1 is a penalty, and w_2 is a weight factor used to give the GCI the same order of magnitude as the error on the workspace. In this work, w_1 = 10000 and w_2 = 30 were chosen. The evaluation of the objective functions in the genetic algorithm is done according to the following steps:

S1. Using the geometrical method, the set of arcs that represent the constant orientation workspace of the manipulator is found.

S2. The area of the error between the prescribed and actual workspaces (α) is computed.

S3. The determinant of $\boldsymbol{J_x}$ for a given working mode is evaluated at consecutive points located on the arcs that define the actual workspace boundary until a sign change of det($\boldsymbol{J_x}$) is found. If no sign change occurs, it is assumed that there are no singularities inside the manipulator workspace for this working mode.

S4. The previous step is repeated for each of the manipulator's eight working modes and the results are assigned to binary variables k_j (k_j = 1 if a sign change is found, k_j = 0 otherwise).

S5. If k_j = 0 for at least one value of j (j = 1,2,…,8), the binary variable representing singularity avoidance is set to 0 (τ = 0). Otherwise, τ = 1.

S6. (used only when Eq. (29) is optimized) The GCI of the manipulator is calculated for each of the working modes that have no corresponding singularities inside the workspace. The variable representing dexterity (β) is set to the highest value of the GCI among those obtained for different working modes.

Both symmetric and non symmetric prescribed workspaces are used in this work. The areas of the symmetric and non symmetric workspaces chosen are 67.98 and 45.75 squared units, respectively. The orientation of the manipulator's mobile platform is set at $\phi = 0$ degrees for all optimizations.

Figure 6 shows the results of an optimization using Eq. (28) for a symmetric prescribed workspace. The geometric and kinematic parameters of this manipulator are listed in Table 2. For this manipulator, there is only one acceptable working mode (AWM) with regard to parallel singularities (Δ_5). It can be observed that the error on the workspace is very small (3% of the area of the prescribed workspace).

The results of an optimization using Eq. (29) as the objective function are presented in Figure 7 and Table 3. It can be seen that, for this manipulator, the error between the prescribed and actual workspaces is slightly higher. However, the optimization of the dexterity yields a higher GCI. This compromise between workspace error and manipulator dexterity is a usual occurrence in the optimization process. The optimized working mode (OWM) with regards to dexterity for this manipulator is Δ_1.

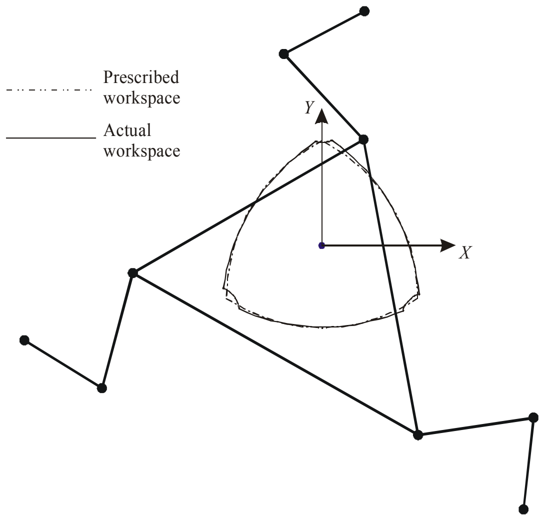

Figure 6 Optimization of manipulator workspace and singularity avoidance (symmetric workspace)

Table 2 Geometric and kinematic parameters : optimization of manipulator workspace and singularity avoidance (symmetric workspace)

B_{1x}	-15.63	B_{1y}	-2.18	P_{1x}	-9.94	P_{1y}	-1.44	l_1	4.73	α	1.88
B_{2x}	10.57	B_{2y}	-10.82	P_{2x}	5.06	P_{2y}	-9.74	l_2	6.08	β	0.29
B_{3x}	2.22	B_{3y}	14.70	P_{3x}	2.20	P_{3y}	5.37			AWM	Δ_5

Results equivalent to those presented above for a symmetric prescribed workspace are also obtained for a non symmetric prescribed workspace. Manipulators optimized using Eqs. (28) and (29) are shown in Figures 8 and 9, respectively. The geometric and kinematic parameters of these manipulators are detailed in Tables 4 and 5.

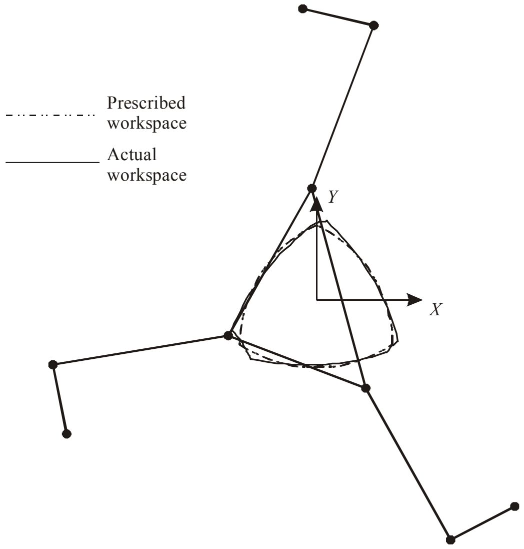

Figure 7 Optimization of manipulator workspace, dexterity and singularity avoidance (symmetric workspace)

Table 3 Geometric and kinematic parameters : optimization of manipulator workspace, dexterity and singularity avoidance (symmetric workspace)

B_{1x}	-16.31	B_{1y}	-6.00	P_{1x}	-5.72	P_{1y}	-2.35	L_1	4.77	α	4.73
B_{2x}	12.98	B_{2y}	-10.89	P_{2x}	3.21	P_{2y}	-5.88	L_2	11.65	β	0.55
B_{3x}	-0.85	B_{3y}	22.60	P_{3x}	-0.27	P_{3y}	7.54			OWM	Δ_1

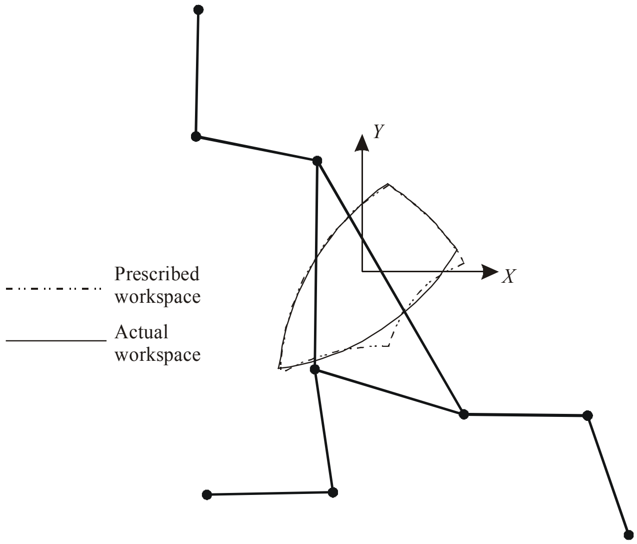

Figure 8 Optimization of manipulator workspace and singularity avoidance (non symmetric workspace)

Table 4 Geometric and kinematic parameters : optimization of manipulator workspace and singularity avoidance (non symmetric workspace)

B_{1x}	-9.24	B_{1y}	-9.35	P_{1x}	-2.39	P_{1y}	-4.99	l_1	6.43	α	2.90
B_{2x}	12.28	B_{2y}	-11.36	P_{2x}	5.18	P_{2y}	-7.24	l_2	6.30	β	0.38
B_{3x}	-9.69	B_{3y}	15.26	P_{3x}	-2.31	P_{3y}	5.60			AWM	Δ_5

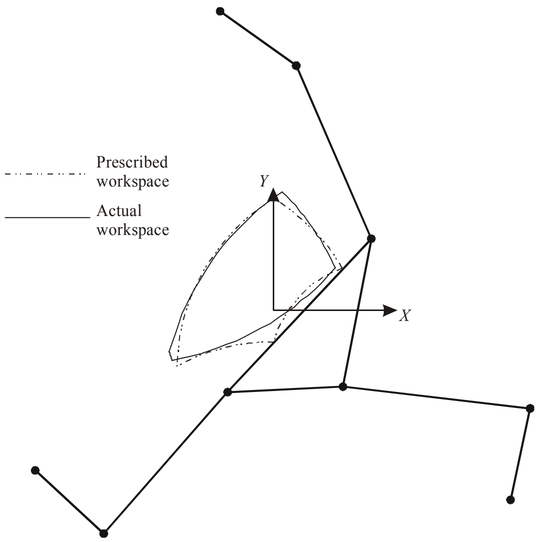

Figure 9 Optimization of manipulator workspace, dexterity and singularity avoidance (non symmetric workspace)

Table 5 Geometric and kinematic parameters : optimization of manipulator workspace, dexterity and singularity avoidance (non symmetric workspace)

B_{1x}	-13.58	B_{1y}	-9.07	P_{1x}	-2.61	P_{1y}	-4.62	l_1	5.29	α	5.88
B_{2x}	13.47	B_{2y}	-10.78	P_{2x}	3.93	P_{2y}	-4.33	l_2	10.72	β	0.52
B_{3x}	-3.03	B_{3y}	16.99	P_{3x}	5.55	P_{3y}	4.05			OWM	Δ_8

In order to gain insight into the consistency of the results generated by the genetic algorithm as well as to better compare the different objective functions, box plots of the workspace error as well as of the GCI are presented in Figures 10 and 11. The samples on which these plots are based consist of a minimum of 30 results obtained for each of the four optimization types: symmetric and non symmetric prescribed workspaces (SW and NSW, respectively) as well as the optimization of workspace error (W), dexterity (D) and singularity avoidance (S).

It can be observed in Figure 10 that the workspace error generated by the genetic algorithm is generally consistent for all optimization types. Furthermore, from Figure 11, the values of the GCI obtained when the dexterity is optimized in the objective function are consistently higher than when it is not. In fact, statistical tests confirm this fact with a 99% confidence level for both symmetric and non symmetric prescribed workspaces.

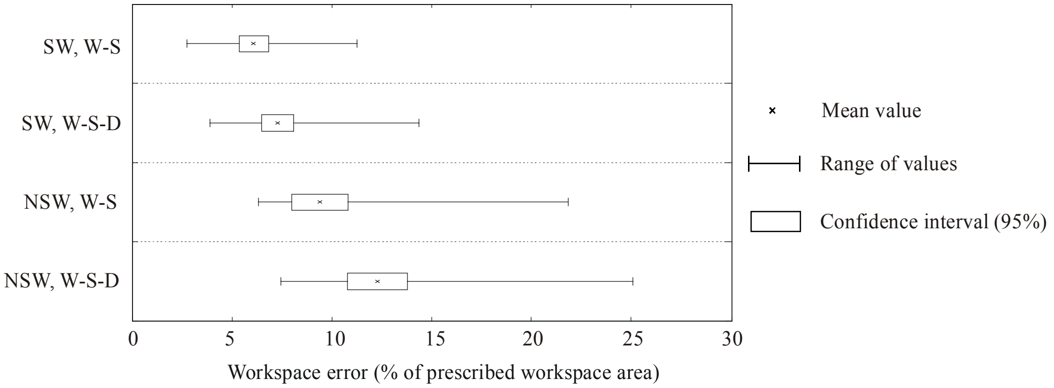

Figure 10 Box plot of workspace error for each of the optimization types

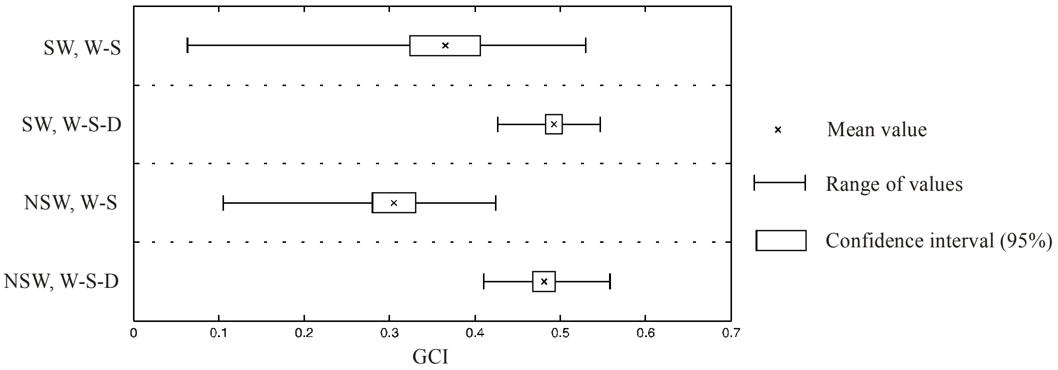

Figure 11 Box plot of GCI for each of the optimization types

9. CONCLUSION

In this work, planar 3-$\underline{R}$RR parallel manipulators were optimized using a genetic algorithm while considering workspace error, dexterity and singularity avoidance as design criteria. Results were obtained for both symmetric and non symmetric prescribed workspaces. It was found that the genetic algorithm produced generally consistent workspace errors for all optimization types. However, the workspace error was compromised slightly when optimizing dexterity. According to the results, it can be stated with a 99% confidence level that the optimization of dexterity produces better conditioned manipulators.

The principle contribution of this work is the development of a design method that is capable of avoiding the presence of parallel singularities inside the workspace of a 3-$\underline{R}$RR manipulator for one or more of its working modes. It was also shown that some 3-$\underline{R}$RR manipulators do not have any parallel singularities (for all working modes) inside their workspace for several orientations of their mobile platform.

Finally, it was observed that the physical size of the optimized manipulators was not affected by the use of different objective functions in the genetic algorithm. A possible addition to the synthesis method proposed here would be to add a parameter representing the ratio of the manipulator size to its workspace area in the genetic algorithm's objective function with the goal of obtaining smaller manipulators.

ACKNOWLEDGEMENTS

The authors wish to thank the NSERC (Natural Science and Engineering Research Council of Canada) for its financial support.

REFERENCES

1. Gosselin, C., Angeles, J., The optimum kinematic design of a planar three-degree-of-freedom parallel manipulator, *ASME Journal of Mechanisms, Transmissions, and Automation in Design*, 110, 35-41, 1988.
2. Murray, A.P., Pierrot, F., Dauchez, P., McCarthy, M., A planar quaternion approach to the kinematic synthesis of a parallel manipulator, *Robotica*, 15(4), 361-365, 1997.
3. Merlet, J.-P., Designing a parallel manipulator for a specific workspace, *The International Journal of Robotics Research*, 16(4), 545-556, 1997.

4. Dibakar, S., Mruthyunjaya, T.S., Synthesis of workspaces of planar manipulators with arbitrary topology using shape representation and simulated annealing, *Mechanism and Machine Theory*, 34, 391-420, 1999.
5. Gosselin, C.M., Wang, J., Singularity loci of planar parallel manipulators with revolute actuators, *Robotics and Autonomous Systems*, 21, 377-398, 1997.
6. Bonev, I.A., Gosselin, C.M., Singularity loci of planar parallel manipulators with revolute Joints, *2nd Workshop on Computational Kinematics*, Seoul, South Korea, 2001.
7. Boudreau, R., Gosselin, C.M., The synthesis of planar parallel manipulators with a genetic algorithm, *ASME Journal of Mechanical Design*, 121, 533-537, 1999.
8. Boudreau, R., Gosselin, C.M., La synthèse d'une plate-forme de Gough-Stewart pour un espace atteignable prescrit, *Mechanism and Machine Theory*, 36, 327-342, 2001.
9. Baron, L., Workspace-based design of parallel manipulators of star topology with a genetic algorithm, *Proceedings of the 2001 ASME Design Engineering Technical Conferences*, Pittsburgh, Pennsylvania, USA, 2001.
10. Gallant, M., Boudreau, R., The synthesis of planar parallel manipulators with prismatic joints for an optimal, singularity-free workspace, *Journal of Robotic Systems*, 19(1), 13-24, 2002.
11. Merlet, J.-P., Gosselin, C.M., Mouly, N., Workspaces of planar parallel manipulators, *Mechanism and Machine Theory*, 33(1), 7-20, 1998.
12. Kumar, V., Characterization of workspaces of parallel manipulators, *ASME Journal of Mechanical Design*, 114, 368-375, 1992.
13. Gosselin, C., Determination of the workspace of 6-DOF parallel manipulators, *Journal of Mechanical Design*, 112, 331-336, 1990.
14. Gosselin, C.M., Guillot, M., The synthesis of manipulators with prescribed workspace, *ASME Journal of Mechanical Design*, 113, 451-455, 1991.
15. Chablat, D., Wenger, P., Working modes and aspects in fully parallel manipulators, *Proceedings of the 1998 IEEE International Conference on Robotics & Automation*, Leuven, Belgium, 1998.
16. Gosselin, C.M., Angeles, J., Singularity analysis of closed-loop kinematic chains, *IEEE Transactions on Robotics and Automation*, 6(3), 281-290, 1990.
17. Dibakar, S, Mruthyunjaya, T.S., A computational geometry approach for determination of boundary of workspaces of planar manipulators with arbitrary topology, *Mechanism and Machine Theory*, 34, 149-169, 1999.
18. Gosselin, C.M., The optimum design of robotic manipulators using dexterity indices, *Robotics and Autonomous Systems*, 9, 213-226, 1992.
19. Kim, S.-G., Three end-effector point coordinate formulation for parallel mechanism robots, *Ph.D. Thesis, Kwangju Institute of Science & Technology*, Republic of Korea 2002.
20. Gosselin, C.M., Angeles, J., A global performance index for the kinematic optimization of robotic manipulators, *ASME Journal of Mechanical Design*, 113, 220-226, 1991.
21. Wright, A.H., Genetic algorithms for real parameter optimization, Foundations of Genetic Algorithms, G.J.E. Rawlins (Editor), Morgan Kaufman, San Mateo, CA, 1991.